Functional Magnetic Waveguides for Magnonics

Arabinda Haldar[1,*] and Adekunle Olusola Adeyeye[2,*]

[1]Department of Physics, Indian Institute of Technology Hyderabad, Kandi 502285, Telangana, India

[2]Department of Physics, Durham University, South Road, Durham, DH1 3LE, United Kingdom

*Corresponding authors: arabinda@phy.iith.ac.in (A. Haldar), adekunle.o.adeyeye@durham.ac.uk (A. O. Adeyeye)

Abstract

Magnonics or spin wave based spintronics is an emerging technology where magnons – quanta for spin waves – process the information analogous to electronic charges in electronics. We introduce the fundamental components of a magnonic device and briefly discuss their electrical control. The magnetic waveguide – an integral part of a magnonic circuit – guides the spin wave signal (magnon current) of desired frequency, wave vector, phase and amplitude which are the key ingredients for wave based computing. Typically, a bias magnetic field aligns magnetization to satisfy anisotropic magnon dispersions for low-energy and long-wavelength magnons and thus, it hinders on-chip device integration capability. We discuss strategies to eliminate the requirements of such a bias field by utilizing self-biased waveguides which are based on either exchange coupled magnetic multi-layer based magnetic micro-wire or dipolar coupled but physically separated chain of rhomboid nanomagnets. We emphasize that the self-biased waveguides offer additional functionalities as compared to conventional waveguides. In this regard, manipulation of spin waves or the gating operation is presented by utilizing

reconfigurable remanent magnetic states of the waveguide externally controlled by field or microwave current. We discuss the prospects of these bias-free waveguide strategies in the rapidly developing field of nano-magnonics and their potential for practical realizations of a magnonic-electronic hybrid technology.

Keywords: Magnonics, Magnetic waveguides, Micro-Brillouin light scattering microscopy, Spin waves, Surface spin waves, Isotropic spin waves, Manipulation of spin waves, Spin wave dispersion, Nano-magnonics, Nanomagnetic devices, Spin wave spectroscopy

INTRODUCTION

Non-charge based technologies are of great interest with growing demand for high frequency information processing and billions of connected devices as conventional semiconductor electronics is reaching its limit.[1–7] It offers unique opportunities for wave-based technologies such as magnonics which is found to be promising for beyond-charge-based current semiconductor electronics.[8–18] It is widely acknowledged that magnonics is a promising candidate for future neuromorphic computing[19–23] and Boolean computing[10,24–26]. In magnonics, the data are encoded in the amplitude or phase of the magnons which are quanta for spin waves – analogous to photons for light waves in photonics. Spin waves represent a phase-coherent collective oscillation of precessing magnetization vectors in a magnetic medium. The wavelength of propagating spin waves or magnon current can be as small as nm which makes them suitable for on-chip device integration in addition to the unparalleled ease of tunability of magnons in comparison to its competitors; photonics or plasmonics.[16,27,28] The heart of a magnonic device is a magnetic waveguide that transmits and processes spin waves. Spin waves have different dispersion characteristics depending on their wavelength and waveguide properties. There are three other major building blocks for a magnonic device: generation, detection and manipulation of the spin waves which can be associated with the input, output and gate, respectively in terms of an electronic device as shown in Fig. 1. Below, we briefly introduce them before discussing the magnetic waveguide which is the main focus of this perspective.

A giant leap towards practical implementation of the magnonic devices has been achieved since the demonstration of spin current to charge current conversion and vice versa.[29–33] The generation of spin current from charge current was achieved by using the spin Hall effect (SHE) where a flow of the electronic charge in heavy metal with a large spin orbit coupling (SOC) strength results in a spin current flow in the orthogonal direction.[34–38] One of the most

important developments in magnonics is the demonstration of a nano-oscillator for the excitation of spin waves using the effect called spin transfer torque (STT) and therefore it is also known as spin torque nano oscillator (STNO).[39–48] Another route for coherent magnon spin current generation is based on spin orbit torque (SOT) mechanism where an auto-oscillation in a nano-confined zone of a magnetic waveguide is achieved by compensating the damping by SOT and it is known as spin Hall nano-oscillator (SHNO).[49–53] On the other hand, electrical detection of spin waves has been realized using the inverse spin Hall effect (ISHE) where the injected spin current in the heavy metal (material with large SOC) generates an orthogonal charge current flow and thereby an electrical voltage.[32,54–56] STT/SOT-based electrical input and ISHE based electrical output open the possibility of nanoscale integration of magnonic devices. Next, the manipulation ('gate' operation) of magnon current requires an external control on the spin waves in the magnetic waveguide in order to achieve a desired signal amplitude/phase at the output.[57–59] The manipulations of spin waves or different logic operations have been demonstrated in several ways based on the modulation of the magnetic properties by optical pulses[60], field inhomogeneity[61,62], interference of spin waves[25,63–66], domain walls[67,68] , spin wave non-reciprocity[69] and reconfigurable magnetic switching[70,71].

Other than the input, output and gate, an integral part of a magnonic device is the magnetic waveguide which supports the propagation of the magnon current. Varieties of magnetic waveguides have been proposed to date in order to access or manipulate different regimes of frequency (f), wavevector (k) and phase of the spin waves.[28,68,70,72–90] The characteristics of the spin waves *i.e.* their dispersion $f(k)$ strongly depends on the material properties, dimensions and shapes of the waveguide. Besides, the choice of the material determines the decay length (λ) – a parameter that represents the length over which the spin wave intensity drops by a factor of e. It is large for materials with low damping properties. One of the primary requirements for a waveguide is to support propagation of coherent spin waves

over a large distance i.e. a large value of λ. Thus, materials with low damping properties are of great importance. Some of the well-known low damping materials known so far are $Y_3Fe_5O_{12}$ (YIG)[91] among the oxides and $Ni_{80}Fe_{20}$ (Permalloy)[85], CoFeB[27], Heusler alloys[92] among metallic materials. Note that these materials are all in-plane magnetized and there are no materials known with perpendicular magnetic anisotropy (PMA) which is suitable as a waveguide for spin wave propagation. Waveguides also allow one to engineer spin wave properties like conversion and splitting of modes.[66,78,80,81,88] Waveguides based on metamaterials known as magnonic crystal – an artificially engineered crystal for the gain of different functions – have been found promising for precise tailoring of the spin wave bands.[93–102] Due to the characteristics of spin wave dispersions (*i.e.* $f(k)$), magnetization (M) of the waveguides needs to be aligned in pre-defined geometry by using an external bias field. Among the various challenges, this requirement of a bias magnetic field (typically 50 – 500 mT) in the magnonic devices possesses a major bottleneck for on-chip device integration capability.[40,84,103] Use of an external bias not only increases the size of the devices but also a huge setback as its stray field could interfere with surrounding devices on the chip. It has led to several attempts to overcome the bias field. The use of magnetic domain walls[67,89] and crafting magnetic domains by using a hot tip of a scanning probe microscope[75] have recently been proposed where bias field is absent and the propagating spin waves have been observed to propagate few-μm distance. In this context, we have recently shown that self-biased magnetic waveguides can be used for the efficient propagation of spin waves.[70,74]

In this brief perspective, we discuss the properties required in designing an efficient and functional waveguide for magnonic devices. Different types of propagating spin wave characteristics and their theoretical model are first introduced. Experimental results based on micro-Brillouin light scattering (μ-BLS) are presented to demonstrate propagating spin waves. Subsequently, recent developments of bias-free magnetic waveguides are discussed. In this

context, first, a waveguide that is designed to support isotropic spin wave propagation is introduced. Next, another waveguide based on the dipolar coupled but physically separated chain of self-biased nanomagnets has been presented. Further, the functionality of this waveguide in terms of the gating of spin waves is discussed. Finally, we put forward our vision for the waveguides on their device integration and functionality. We believe that the results will demonstrate the potential of bias-free waveguides for future magnonic device based information processing.

THEORETICAL MODEL FOR SPIN WAVES IN MAGNETIC WAVEGUIDES

The focus of this perspective is the magnetic waveguide of a magnonic device. In order to understand the strategies for making the waveguides efficient and functional, we have briefly described the spin wave propagation characteristics in typical waveguide structures and their theoretical model. Magnetization dynamics are governed by several interactions (exchange, anisotropy, demagnetization, and Zeeman) in a magnetic system which is represented by an effective field, H_{eff}. The precession of magnetization (M) around the H_{eff} is described by the famous Landau-Lifshitz-Gilbert (LLG) equation,[104,105]

$$\frac{d\boldsymbol{M}}{dt} = -\gamma\mu_0\left(\boldsymbol{M} \times \boldsymbol{H}_{eff}\right) + \frac{\alpha}{M_S}\left(M \times \frac{d\boldsymbol{M}}{dt}\right)$$

where γ, μ_0, α and M_S are the gyromagnetic ratio, vacuum permeability, Gilbert damping and saturation magnetization, respectively. In the limit of small excitation, the LLG equation can be linearized and dependence of spin wave oscillation frequency ($\omega = 2\pi f$) to the wavevector (k), i.e. the magnon dispersion ($\omega(k)$) can be obtained. The details of the theoretical development can be found elsewhere.[106–110] In the case of waveguides structured in micron or sub-micron sizes, the magnon dispersions are significantly different as compared to that of the magnetic thin films. This effect is more prominent when the lateral dimension of the

waveguides is comparable to the wavelength of the magnons which is the case in nano-magnonic devices. A schematic of such a micro-structured waveguide (width = *w* and thickness = *d*) is shown in Fig. 2(a) where the length is much larger than the width. Magnon current propagates along the length of the waveguide i.e. *x*-axis is considered as propagation co-ordinate. As shown in Fig. 2(a), ϕ is the angle between $\boldsymbol{M}$ and the film normal (*z*-axis) and θ_M is the angle between $\boldsymbol{M}$ and $\boldsymbol{k}$ or propagation coordinate (*i.e. x*-axis). Spin waves are quantized along the width of the waveguide which is denoted by a mode number *n* and a corresponding wavevector, k_n. A concept of effective width (w_{eff}) is introduced to account for the non-uniform demagnetization field near the edge of the width of the waveguide.[111] It can be described as: $w_{eff} = w[U/(U-2)]$; where $U(\beta) = 2\pi/\beta[1 + 2ln(1/\beta)]$ and $\beta = d/w$. Therefore, the total wavevector (k_{tot}) is defined as $k_{tot}^2 = k^2 + k_n^2$, where $k_n = n\pi/w_{eff}$. In such a geometry (assuming $\beta \ll 1$), the magnon dispersion can be described as:[10]

$$f_n = \sqrt{(f_0 + f_M l_{ex} k_{tot}^2)(f_0 + f_M l_{ex} k_{tot}^2 + f_M F)}$$

where, $f_0 = (\gamma/2\pi)\mu_0 H_0$, $f_M = (\gamma/2\pi)\mu_0 M_S$ (in the weak excitation approximation), l_{ex} is the exchange length, M_S is the saturation magnetization, H_0 is the effective magnetic field and the parameter F is defined as:

$$F = P + sin^2\phi \times \left(1 - P\left(1 + cos^2(\theta_k - \theta_M)\right) + \frac{f_M P(1-P) sin^2(\theta_k - \theta_M)}{f_0 + f_M l_{ex} k_{tot}^2}\right)$$

where $P = 1 - (1 - e^{-dk_{tot}})/dk_{tot}$ and $\theta_k = arctan\,(k_n/k)$. Three types of spin waves are defined based on the magnon propagation direction ($\boldsymbol{k}$) with respect to the external magnetic field ($\boldsymbol{H_a}$), thereby the magnetization ($\boldsymbol{M}$). These three types of spin waves are known as Damon-Eshbach[112] (DE) or surface waves for $(\phi, \theta_M) = (90°, 90°)$, backward volume (BV) waves for $(\phi, \theta_M) = (90°, 0°)$ and forward volume (FV) waves for $(\phi, \theta_M) = (0°, 90°)$. Thus,

we have two types of spin waves (BV and DE or surface waves) for the in-plane magnetized waveguides and FV spin waves are for the perpendicularly magnetized waveguides.

μ-BLS EXPERIMENT

In order to experimentally detect the magnon current and its characteristics, here we have discussed μ-BLS technique which is the best-known tool for local spin wave measurements and spatial imaging. A simplified schematic of this experiment is shown in Fig. 2(b). A monochromatic 532-nm green laser is focused by using a ×100 microscope objective with a large numerical aperture. It enables a diffraction-limited laser spot diameter of around 250 nm. The sample is placed on top of a nano-positioning stage in order to scan the laser spot for spatial resolution and the long-term stabilization was achieved by an active-feedback algorithm. The scattered laser beam from the sample is measured using a tandem Fabry-Perot interferometer. More details on the μ-BLS technique can be found elsewhere.[113–115] Magnon current is generated in magnetic waveguides by using a ground-signal-ground (G-S-G) style microwave antenna in the range of 0−20 GHz frequency. Note that the width (b) of the antenna which is 1 μm in the following results, sets an upper limit to the generated magnon wavevector: $k_{max} = 2\pi/b = 6.2\, rad/\mu m$.[116]

EXAMPLES OF TYPICAL MAGNETIC WAVEGUIDES AND THEIR LIMITATIONS

First, we discuss the BV spin waves in a typical Py waveguide structure (w = 2 μm, d = 5 nm) fabricated using lithography techniques (optical and electron-beam) as shown in Fig. 2(c). The antenna for spin wave excitation was made from 70-nm-thick and 1-μm-wide Au. Details of the device fabrication can be found elsewhere.[74] Note that magnetization points along the length of the waveguide at remanence in such micro-wire structures and therefore BV geometry ($\boldsymbol{M} \parallel \boldsymbol{k}$) is realized without any bias magnetic field (H_a = 0). BLS spectra at the remanent state of the waveguide are shown in Fig. 2(d) which shows some spin wave response

only near 1.9 GHz. Calculated BV dispersion (for n = 1 and H_a =0) using the dispersion equation as mentioned above is shown in Fig. 2(e) by assuming the standard parameters for Py: M_S = 8×10^5 A/m, exchange constant, A = 13×10^{-12} J/m which is related to l_{ex} as: $l_{ex} = \sqrt{(2A/\mu_0 M_S^2)}$. The dotted line in Fig. 2(e) refers to the k_{max} that can be excited by the 1-µm-wide antenna. Dispersion plot reveals that any propagating ($k \neq 0$) BV modes should have frequencies lower than 1.8 GHz at k = 0. Thus, the model is consistent with the experiment and a slight mismatch may be due to the use of standard parameters for Py instead of the actual values of this sample. Nevertheless, any low damping in-plane magnetic material is suitable for the investigation of BV waves.[117] However, BV waves have negative group velocity and do not propagate long distances in micro-structured waveguides.[118] BV waves have been used in a variety of applications like parametric excitation of spin waves[94,119,120] and logic gates[24,66].

On the other hand, to realize DE or surface spin waves ($\boldsymbol{M} \perp \boldsymbol{k}$), the 2-µm-wide waveguide needs to be magnetized along its short (hard) axis and therefore a large bias field is typically applied as shown in the schematic in Fig. 2(f). BLS spectra for such DE waves are shown at three different external magnetic fields (H_a = 60, 90, 120 mT) in Fig. 2(g). DE spin wave dispersions are calculated using the above-mentioned equation for n = 1. The wavevector of the experimental DE modes can be extracted by analyzing the calculated dispersion plot in Fig. 2(h). Note that the DE or the surface spin waves are the typical choice for any magnonic device prototype.[28,70,72,73,75,76,78–80,85–89] This is due to the strong intensity of the DE spin waves at the surface of the waveguide which makes them suitable for integration with electrical input or output.[40] Moreover, the surface spin waves can be efficiently excited using a microwave antenna due to the orthogonal alignment between the RF excitation field (h_{rf}) and the magnetization orientation which maximizes the torque ($\boldsymbol{M} \times \boldsymbol{h_{rf}}$). We would also like to point here that the bias field value will significantly increase with a decrease of the waveguide width due to the large demagnetization field. Thus, an alternative approach for waveguide design that

eliminates the requirement of such a large bias field is highly desired in nano-magnonic devices.

Next, we discuss the third type, *i.e.* the FV spin waves ($\boldsymbol{M} \perp \boldsymbol{k}$) that have isotropic propagation in the plane of the film and the magnetization in the out-of-plane (OOP) direction. As noted above, all the low damping materials, well-known for their long magnon propagation length are all in-plane magnetized and there are yet no examples of low-damping magnetic materials which has PMA. Therefore, to achieve a FV geometry that is suitable for isotropic spin wave transport, one needs to apply an even larger field to achieve OOP magnetization in comparison to the field in DE configuration as discussed earlier.[121,122] Moreover, there are constraints in the device geometry and subsequent measurements in the presence of an OOP field. Therefore, there no experimental reports on FV spin waves in patterned magnetic waveguide structures. However, owing to isotropic propagation characteristics FV spin wave-based logic devices are found to be more efficient than the other two waves in terms of designing complex magnonic circuits proposed using micromagnetic simulations.[22,103] Note here that exchange magnons (high energy and small wavelength magnons) have also isotropic propagation characteristics and they are promising for the miniaturization of the magnonic devices down to the nanoscale. Exchange magnons can be excited in different ways, e.g. spin Hall effect[123], parametric excitation[119,124], spin Seebeck effect[125], or waveguide designs[28]. However, it is simpler to excite/manipulate low energy magnons with long wavelengths and here we discuss our recent works on such spin waves.

BIAS-FREE WAVEGUIDE FOR ISOTROPIC SPIN WAVE PROPAGATION

We have demonstrated a magnetic waveguide where a well-known in-plane material, Py is forced to align in the OOP direction without any bias magnetic field.[74] This was achieved by depositing a thin Py film (5-nm-thick) directly on top of a strong PMA multilayer stack:

$[Co(0.3)/Pd(1.1)]_6$, henceforth Co-Pd. The number in the first brackets represents the thickness in nm and the repetition of the Co/Pd multilayer is 6. When a Py film is placed on top of the Co-Pd the exchange coupling strength of the OOP magnetized Co-Pd forces 5-nm-thick Py in the OOP direction. Here, the thickness of the Py layer is crucial. A thicker Py might have exchange spring-like magnetic orientation across the Py thickness as the exchange coupling strength decreases away from the interface. Few-micron-wide magnetic waveguides are lithographically fabricated of from a multilayer stack of $Cr(5)/Cu(10)/Pd(5)/[Co(0.3)/Pd(1.1)]_6/Py(5)$; henceforth Co-Pd-Py. The details of the fabrications can be found elsewhere.[74] In order to excite spin waves in this waveguide, a 1-µm-wide Au antenna was placed on top of the waveguide using electron beam lithography and lift-off process. Spin waves have been detected using the µ-BLS technique. An optical image of the sample geometry obtained from the µ-BLS sample visualization/stabilization camera is shown in Fig. 3(a). Shown in Fig. 3(b) are the OOP hysteresis loops that have been measured by using a focused magneto-optical Kerr effect (MOKE) technique which is sensitive to the top surface. It is evident from Fig. 3(b) that Co-Pd-Py has OOP magnetization at remanence with almost a square hysteresis loop with a large coercive field value ($\mu_0 H_c$ ~ 118 mT). Note that we have found a much higher coercive field ($\mu_0 H_c$ ~ 240 mT) for Co-Pd multilayer without the Py layer. Propagating spin waves have been recorded at remanence (*i.e.* H_a = 0) away from the antenna and the prominent responses were found below 6.5 GHz (Fig. 3(c)). Figure 3(d) shows the exponential decay of the spin wave intensity which is fitted to $\exp(-2x/\lambda)$, that reveals λ ~ 2 µm. In order to show the isotropic propagation, a concept waveguide with three channels oriented at arbitrary angles have been lithographically fabricated as shown in Fig. 3(e). BLS spectra recorded in these three channels confirms the propagating modes at 5.7, 6.7 and 8.2 GHz. Spatial profiles of the spin wave propagation have been imaged experimentally by scanning the laser spot over the shaded region as shown in Fig. 3(e). Two dimensional (2D)

spatial maps of the spin wave intensity show the propagation of spin wave in all the channels which are at different angles with respect to the antenna (Fig. 3(f)). Note that all the spin wave measurements were carried out without any bias. Thus, exchange coupled Py waveguide offers a solution for the realization bias free FV isotropic waves – crucial for magnonic circuit designs.

BIAS-FREE WAVEGUIDE WITH RECONFIGURABLE DEFECT FOR SURFACE SPIN WAVE PROPAGATION AND MANIPULATION

Next, we focus on the DE or surface spin waves which are the most exploited in the magnonic devices and we discuss a solution for their prorogation without any bias magnetic field. A special type of magnetic waveguide has been designed based on the dipolar coupled but physically separated chain of rhomboid-shaped nanomagnets (RNMs).[70] The device schematic is shown in Fig. 4(a) and the scanning electron microscopy (SEM) image of the device is shown in Fig. 4(b). The nanomagnets have a width and length of 260 nm and 600 nm, respectively. The special shape of the nanomagnet enables unique magnetic orientation when initialized along their short axes in contrast to a simple rectangular nanomagnet. This is due to a slight difference between the geometrical short axis and magnetic hard axis which leads to a preferential orientation when biased along their short axes. More details about the operation of the rhomboid nanomagnet can be found elsewhere.[126,127] The small separation (50 nm) between the nanomagnets in the waveguide ensures strong dipolar coupling. When spin waves are excited in the nanomagnets underneath the 80-nm-thick antenna (where *rf* field intensity is maximum), it also propagates through the waveguide away from the antenna. Prior to any spin wave measurements, we initialize all the nanomagnets along their long axis followed by removal of the field (H_I : 1000 Oe $\rightarrow$ 0). It ensures all the magnets point in the same directions as shown in the magnetic force microscopy (MFM) image in Fig. 4(d) and this remanent state is referred as ferromagnetically ordered (FO) state. Propagating spin waves at a distance away

from the antenna are measured by using μ-BLS laser spot (marked as 'output' in Fig. 4(b)) and the spectra are shown in Fig. 4(c). A strong propagating spin wave mode is observed at 4.2 GHz for the FO state. We have found $\lambda \sim 1$ μm by analyzing the spatial profile of the spin wave propagation by scanning the laser spot over the waveguide. Thus, bias-free surface waves have been realized using this special type of waveguide. Another successful waveguide strategy is based on magnetic domain walls which support DE spin waves without a bias.[67,75,89]

One of the primary elements of a magnonic device is the manipulation or gating of the magnon current. We showed the gating operation based on switching a nanomagnet which was oriented differently using lithography technique as marked by 'gate' in Fig. 4(b). The magnet at the gate position aligns opposite to the rest of the nanomagnets in the waveguide when initialized along the short axes of the nanomagnets. Shown in Fig. 4(f) is an MFM image indicating this opposite orientation at the gate position and this state is referred to as FO*. Subsequently, spin wave response is recorded at the output position and the intensity of the spin waves at 4.2 GHz is drastically reduced (Fig. 4(c)). Interestingly, the 2D spatial profile (Fig. 4(g)) of the spin waves shows an absence of the spin wave response at the gate position and a reduced spin wave intensity beyond the gate position in comparison to the FO state. We have found the reflection, interference and transmission properties of the spin waves at the defect position and the results are consistent with previous observations in the typical waveguides.[61,86,87] Note that all the measurements were conducted at remanence and the field was only used to reconfigure the waveguide between FO and FO* states. For practical implementation, one can utilize cross-point current lines for Oersted field induced reconfiguration.

SURFACE SPIN WAVE PROPAGATION ACROSS A BEND WITHOUT ANY BIAS

Next, we address another bottleneck for the DE spin waves which is the transmission around a bend in a waveguide. Typically, DE spin waves are achieved by saturating a magnetic waveguide along its short axis. However, a global bias field does not satisfy DE geometry in a curved waveguide which might be required for circuit implementations. Magnetic domain walls[89] and current-induced Oersted field[72,73] have been proposed in order to overcome this challenge in the past. Note that the use of bias current leads to Joule heating which hinders the advantages promised by magnonics. Here, in our RNM based waveguide design, this issue is simply resolved by placing the nanomagnets at an angle (for example 32°) as shown in Fig. 4(h). As the magnets are self-biased and initialized along their long axes, DE geometry is satisfied throughout the waveguide even without applying any field. The propagation of spin waves can be seen from the measured 2D spatial profiles of the spin waves at 5.1 GHz around the bend as shown in Fig. 4(i).

WAVEGUIDE FOR MICROWAVE-ASSISTED GATING OF SURFACE SPIN WAVES

Furthermore, we have discussed a different gating technique that simplifies further the device operation. We utilize a similar type of waveguide design using coupled RNM-based waveguide and we showed that one can control the flow of magnon current by using a microwave current.[71] Here, a waveguide is designed where all the RNMs have the same geometrical orientation. The magnon current is excited using an antenna (input) made from 80-nm-thick Pt. The manipulation (gate) of the magnon current flow is achieved by using the same excitation antenna but with large microwave power. We have measured the magnon signal using μ-BLS technique at a distance away from the antenna as shown by a green circular dot in Fig. 5(a). The magnon spectra reveal that the waveguide has a strong propagating spin wave mode at 4.2 GHz. In order to show the control of the magnon current flow, first, the waveguide was initialized by using an external magnetic field along the long axis of the RNMs followed

by removal of the field. It ensures all the nanomagnets in the waveguide have the same magnetic orientation at remanence. Subsequently, the waveguide at remanence was initialized with a microwave current with different powers from 10 mW to 100 mW which is referred to as initialization power for a couple of seconds prior to the recording of the BLS spectra. Magnon spectra were recorded at 4.2 GHz without applying any external magnetic field (*i.e.* remanent state of the waveguide) for three different excitation power ($P_{exc.}$ = 1, 3 & 10 mW) and the results are shown in Fig. 5(b). The results show a drastic reduction of the spin wave intensity above an initialization power of ~ 45 mW. High and low intensity regions i.e. below and above 45 mW are labeled as region I and region II, respectively in the following discussion. Representative full BLS spectra for these two regions are shown in Fig. 5(c). Further, such variation was confirmed by performing 2D spatial scan of the BLS laser spot at these two regions as shown in Fig. 5(d-e). The underlying mechanism of this manipulation of spin wave signal using microwave current is attributed to the switching of the nanomagnets at region II *i.e.* during the initialization process with high microwave power (> 45 mW). Note that the oscillating microwave magnetic field is maximum just underneath the antenna and it is directed along the short axes of the RNMs. Therefore, when we focus on the nanomagnets underneath the antenna using the MFM technique (Fig. 5(e-f)), we see a difference in the MFM contrasts indicating magnetization switching in region II. The results are also consistent with the fact that we should expect a reduced spin wave intensity when one or more nanomagnets are switched in the waveguide as discussed in the earlier section. Note that the original magnetic state of the waveguide is restored by applying an initialization field along the short axis of the waveguide. Thus, a new route for the magnon gating was achieved using the same input antenna which is typically used only to generate magnon current. This device scheme can thereby eliminate the requirement of a separate gate contact pad, thereby a possibility of simplifying the magnonic circuit further.

OUTLOOK

There are several outstanding challenges to address for magnonic devices to be competitive and/or compatible with existing semiconductor-based microelectronics. Here, we provide a summary and progress in the design of efficient magnetic waveguides in particular. The use of an external bias magnetic field remains a major concern as it appears to be unavoidable. Our proposals for bias-field-free magnetic waveguides are therefore a step forward towards the practical realizations of magnonic devices. We show the importance of the self-biased nanomagnets driven via shape-induced anisotropy and engineering the magnetic coupling in a multilayer structure for the realization of bias-free device operation. Moreover, such self-biased waveguides offer additional functionality like the ease of gating operation or transmitting a signal around a corner which were not accessible in a regular magnetic waveguide. Furthermore, downscaling of these waveguides is feasible for nano-magnonics applications and one may harness additional functionalities based on non-linear spin wave physics which is pronounced at the nanoscale.[128] Therefore, it will be of great future interest to explore such bias-free magnetic waveguides along with the nanoscale electrical input and output terminal which utilizes STNO/SHNO and ISHE, respectively. Such integration may pose great challenges, however, it may lead to new opportunities as spin wave properties strongly depend on the device geometry and dimensions. The other available option for self-biased waveguides based on domain walls also needs to be exploited in this context. Next, the waveguide can be made more efficient in terms of larger decay length by the appropriate choice of low damping materials or by compensating for the damping using SOT[129] or SHE[130–132]. Another interesting part of the wave based computation is the utilization of the phase and these bias-free waveguides might offer additional functionality based on phase-based operations. We believe that the proposed design principles for the bias-free magnetic waveguides will provide

a new horizon for nano-magnonics with a step forward for its suitability in device integration and realization of a hybrid magnonic-electronic technology in near future.

ACKNOWLEDGMENTS

A.H. would like to thank the funding under Ramanujan Fellowship (SB/S2/RJN-118/2016), Department of Science and Technology (DST), India. AOA would like to acknowledge the funding from the Royal Society and Wolfson Foundation.

DATA AVAIALABILITY STATEMENT

Data sharing is not applicable to this article as no new data were created or analyzed in this study.

REFERENCES

[1] A. Barman, G. Gubbiotti, S. Ladak, A.O. Adeyeye, M. Krawczyk, J. Gräfe, C. Adelmann, S. Cotofana, A. Naeemi, V.I. Vasyuchka, B. Hillebrands, S.A. Nikitov, H. Yu, D. Grundler, A. Sadovnikov, A.A. Grachev, S.E. Sheshukova, J.-Y. Duquesne, M. Marangolo, C. Gyorgy, W. Porod, V.E. Demidov, S. Urazhdin, S. Demokritov, E. Albisetti, D. Petti, R. Bertacco, H. Schulteiss, V. V Kruglyak, V.D. Poimanov, A.K. Sahoo, J. Sinha, H. Yang, M. Muenzenberg, T. Moriyama, S. Mizukami, P. Landeros, R.A. Gallardo, G. Carlotti, J.-V. Kim, R.L. Stamps, R.E. Camley, B. Rana, Y. Otani, W. Yu, T. Yu, G.E.W. Bauer, C.H. Back, G.S. Uhrig, O. V Dobrovolskiy, S. van Dijken, B. Budinska, H. Qin, A. Chumak, A. Khitun, D.E. Nikonov, I.A. Young, B. Zingsem, and M. Winklhofer, J. Phys. Condens. Matter (2021).

[2] E.Y. Vedmedenko, R.K. Kawakami, D.D. Sheka, P. Gambardella, A. Kirilyuk, A. Hirohata, C. Binek, O. Chubykalo-Fesenko, S. Sanvito, B.J. Kirby, J. Grollier, K. Everschor-Sitte, T. Kampfrath, C.-Y. You, and A. Berger, J. Phys. D. Appl. Phys. **53**, 453001 (2020).

[3] B. Dieny, I.L. Prejbeanu, K. Garello, P. Gambardella, P. Freitas, R. Lehndorff, W. Raberg, U. Ebels, S.O. Demokritov, J. Akerman, A. Deac, P. Pirro, C. Adelmann, A. Anane, A. V. Chumak, A. Hirohata, S. Mangin, S.O. Valenzuela, M.C. Onbaşlı, M. d'Aquino, G. Prenat, G. Finocchio, L. Lopez-Diaz, R. Chantrell, O. Chubykalo-Fesenko, and P. Bortolotti, Nat. Electron. **3**, 446 (2020).

[4] P. Minzioni, C. Lacava, T. Tanabe, J. Dong, X. Hu, G. Csaba, W. Porod, G. Singh, A.E. Willner, A. Almaiman, V. Torres-Company, J. Schröder, A.C. Peacock, M.J. Strain, F. Parmigiani, G. Contestabile, D. Marpaung, Z. Liu, J.E. Bowers, L. Chang, S. Fabbri, M.R. Vázquez, V. Bharadwaj, S.M. Eaton, P. Lodahl, X. Zhang, B.J. Eggleton, W.J. Munro, K. Nemoto, O. Morin, J. Laurat, and J. Nunn, J. Opt. **21**, 63001 (2019).

[5] M.I. Stockman, K. Kneipp, S.I. Bozhevolnyi, S. Saha, A. Dutta, J. Ndukaife, N. Kinsey, H.

Reddy, U. Guler, V.M. Shalaev, A. Boltasseva, B. Gholipour, H.N.S. Krishnamoorthy, K.F. MacDonald, C. Soci, N.I. Zheludev, V. Savinov, R. Singh, P.G.C. Lienau, M. Vadai, M.L. Solomon, D.R. Barton, M. Lawrence, J.A. Dionne, S. V Boriskina, R. Esteban, J. Aizpurua, X. Zhang, S. Yang, D. Wang, W. Wang, T.W. Odom, N. Accanto, P.M. de Roque, I.M. Hancu, L. Piatkowski, N.F. van Hulst, and M.F. Kling, J. Opt. **20**, 43001 (2018).

[6] D. Brunner, M.C. Soriano, C.R. Mirasso, and I. Fischer, Nat. Commun. **4**, 1364 (2013).

[7] E. Ozbay, Science (80-.). **311**, 189 (2006).

[8] A.V. V. Chumak, V.I.I. Vasyuchka, A.A.A. Serga, and B. Hillebrands, Nat. Phys. **11**, 453 (2015).

[9] A. Hirohata, K. Yamada, Y. Nakatani, L. Prejbeanu, B. Diény, P. Pirro, and B. Hillebrands, J. Magn. Magn. Mater. **509**, 166711 (2020).

[10] A. Mahmoud, F. Ciubotaru, F. Vanderveken, A. V. Chumak, S. Hamdioui, C. Adelmann, and S. Cotofana, J. Appl. Phys. **128**, 161101 (2020).

[11] S. Neusser and D. Grundler, Adv. Mater. **21**, 2927 (2009).

[12] B. Lenk, H. Ulrichs, F. Garbs, and M. Münzenberg, Phys. Rep. **507**, 107 (2011).

[13] A. V Chumak and H. Schultheiss, J. Phys. D. Appl. Phys. **50**, 300201 (2017).

[14] A.A.A. Serga, A.V. V. Chumak, and B. Hillebrands, J. Phys. D. Appl. Phys. **43**, 264002 (2010).

[15] V.V. V. Kruglyak, S.O.O. Demokritov, and D. Grundler, J. Phys. D. Appl. Phys. **43**, 264001 (2010).

[16] D. Grundler, Nat Phys **11**, 438 (2015).

[17] A. Haldar and A.O. Adeyeye, J. Appl. Phys. **128**, 240902 (2020).

[18] S.O. Demokritov, Spin Wave Confin. Second Ed. Propagating Waves, Second Ed. **322**, 1 (2017).

[19] T. Brächer and P. Pirro, J. Appl. Phys. **124**, 152119 (2018).

[20] S. Fukami and H. Ohno, J. Appl. Phys. **124**, 151904 (2018).

[21] A. Papp, W. Porod, and G. Csaba, arXiv:2012.04594v1 (2020).

[22] Q. Wang, A. V Chumak, and P. Pirro, Nat. Commun. **12**, 2636 (2021).

[23] Q. Wang, A. Hamadeh, R. Verba, V. Lomakin, M. Mohseni, B. Hillebrands, A. V Chumak, and P. Pirro, Npj Comput. Mater. **6**, 192 (2020).

[24] T. Fischer, M. Kewenig, D.A. Bozhko, A.A. Serga, I.I. Syvorotka, F. Ciubotaru, C. Adelmann, B. Hillebrands, and A.V. Chumak, Appl. Phys. Lett. **110**, 152401 (2017).

[25] M.P. Kostylev, A.A. Serga, T. Schneider, B. Leven, and B. Hillebrands, Appl. Phys. Lett. **87**, 153501 (2005).

[26] A. Khitun and K.L. Wang, J. Appl. Phys. **110**, 34306 (2011).

[27] H. Yu, R. Huber, T. Schwarze, F. Brandl, T. Rapp, P. Berberich, G. Duerr, and D. Grundler, Appl. Phys. Lett. **100**, 262412 (2012).

[28] C. Liu, J. Chen, T. Liu, F. Heimbach, H. Yu, Y. Xiao, J. Hu, M. Liu, H. Chang, T. Stueckler, S. Tu, Y. Zhang, Y. Zhang, P. Gao, Z. Liao, D. Yu, K. Xia, N. Lei, W. Zhao, and M. Wu, Nat. Commun. **9**, 738 (2018).

[29] E. Saitoh, M. Ueda, H. Miyajima, and G. Tatara, Appl. Phys. Lett. **88**, 182509 (2006).

[30] T. Kimura, Y. Otani, T. Sato, S. Takahashi, and S. Maekawa, Phys. Rev. Lett. **98**, 156601 (2007).

[31] T. Seki, Y. Hasegawa, S. Mitani, S. Takahashi, H. Imamura, S. Maekawa, J. Nitta, and K.

Takanashi, Nat. Mater. **7**, 125 (2008).

[32] Y. Kajiwara, K. Harii, S. Takahashi, J. Ohe, K. Uchida, M. Mizuguchi, H. Umezawa, H. Kawai, K. Ando, K. Takanashi, S. Maekawa, and E. Saitoh, Nature **464**, 262 (2010).

[33] L. Liu, C.F. Pai, Y. Li, H.W. Tseng, D.C. Ralph, and R.A. Buhrman, Science (80-.). **336**, 555 (2012).

[34] J.E. Hirsch, Phys. Rev. Lett. **83**, 1834 (1999).

[35] J. Sinova, D. Culcer, Q. Niu, N.A. Sinitsyn, T. Jungwirth, and A.H. MacDonald, Phys. Rev. Lett. **92**, 126603 (2004).

[36] S.O. Valenzuela and M. Tinkham, Nature **442**, 176 (2006).

[37] T. Tanaka, H. Kontani, M. Naito, T. Naito, D.S. Hirashima, K. Yamada, and J. Inoue, Phys. Rev. B - Condens. Matter Mater. Phys. **77**, 165117 (2008).

[38] A. Hoffmann, IEEE Trans. Magn. **49**, 5172 (2013).

[39] M. Madami, S. Bonetti, G. Consolo, S. Tacchi, G. Carlotti, G. Gubbiotti, F.B. Mancoff, M.A. Yar, and J. Åkerman, Nat. Nanotechnol. **6**, 635 (2011).

[40] S. Urazhdin, V.E. Demidov, H. Ulrichs, T. Kendziorczyk, T. Kuhn, J. Leuthold, G. Wilde, and S.O. Demokritov, Nat. Nanotechnol. **9**, 509 (2014).

[41] V.E. Demidov, S. Urazhdin, and S.O. Demokritov, Nat. Mater. **9**, 984 (2010).

[42] F. Macià, A.D. Kent, and F.C. Hoppensteadt, Nanotechnology **22**, 95301 (2011).

[43] M.R. Pufall, W.H. Rippard, S.E. Russek, S. Kaka, and J.A. Katine, Phys. Rev. Lett. **97**, 87206 (2006).

[44] S. Kaka, M.R. Pufall, W.H. Rippard, T.J. Silva, S.E. Russek, and J.A. Katine, Nature **437**, 389 (2005).

[45] D. Houssameddine, U. Ebels, B. Delaët, B. Rodmacq, I. Firastrau, F. Ponthenier, M. Brunet, C. Thirion, J.-P. Michel, L. Prejbeanu-Buda, M.-C. Cyrille, O. Redon, and B. Dieny, Nat. Mater. **6**, 447 (2007).

[46] W.H. Rippard, M.R. Pufall, S. Kaka, S.E. Russek, and T.J. Silva, Phys. Rev. Lett. **92**, 27201 (2004).

[47] S.I. Kiselev, J.C. Sankey, I.N. Krivorotov, N.C. Emley, R.J. Schoelkopf, R.A. Buhrman, and D.C. Ralph, Nature **425**, 380 (2003).

[48] H. Ulrichs, V.E. Demidov, S.O. Demokritov, and S. Urazhdin, Appl. Phys. Lett. **100**, 162406 (2012).

[49] H. Fulara, M. Zahedinejad, R. Khymyn, A.A. Awad, S. Muralidhar, M. Dvornik, and J. Åkerman, Sci. Adv. **5**, eaax8467 (2019).

[50] B. Divinskiy, V.E. Demidov, S. Urazhdin, R. Freeman, A.B. Rinkevich, and S.O. Demokritov, Adv. Mater. **30**, 1802837 (2018).

[51] V.E. Demidov, S. Urazhdin, A. Anane, V. Cros, and S.O. Demokritov, J. Appl. Phys. **127**, 170901 (2020).

[52] V.E. Demidov, S. Urazhdin, G. de Loubens, O. Klein, V. Cros, A. Anane, and S.O. Demokritov, Phys. Rep. **673**, 1 (2017).

[53] R.H. Liu, W.L. Lim, and S. Urazhdin, Phys. Rev. Lett. **110**, 147601 (2013).

[54] A.V. Chumak, A.A. Serga, M.B. Jungfleisch, R. Neb, D.A. Bozhko, V.S. Tiberkevich, and B. Hillebrands, Appl. Phys. Lett. **100**, 082405 (2012).

[55] O. Mosendz, V. Vlaminck, J.E. Pearson, F.Y. Fradin, G.E.W. Bauer, S.D. Bader, and A. Hoffmann, Phys. Rev. B - Condens. Matter Mater. Phys. **82**, 214403 (2010).

[56] S.J. Wang, D. Venkateshvaran, M.R. Mahani, U. Chopra, E.R. McNellis, R. Di Pietro, S. Schott, A. Wittmann, G. Schweicher, M. Cubukcu, K. Kang, R. Carey, T.J. Wagner, J.N.M. Siebrecht, D.P.G.H. Wong, I.E. Jacobs, R.O. Aboljadayel, A. Ionescu, S.A. Egorov, S. Mueller, O. Zadvorna, P. Skalski, C. Jellett, M. Little, A. Marks, I. McCulloch, J. Wunderlich, J. Sinova, and H. Sirringhaus, Nat. Electron. **2**, 98 (2019).

[57] A. Khitun, M. Bao, and K.L.K.L. Wang, J. Phys. D. Appl. Phys. **43**, 264005 (2010).

[58] S.-K.S.K. Kim, J. Phys. D. Appl. Phys. **43**, 264004 (2010).

[59] A. Khitun, M. Bao, and K.L. Wang, IEEE Trans. Magn. **44**, 2141 (2008).

[60] M. Vogel, A.V. Chumak, E.H. Waller, T. Langner, V.I. Vasyuchka, B. Hillebrands, and G. Von Freymann, Nat. Phys. **11**, 487 (2015).

[61] S.O. Demokritov, A.A. Serga, A. André, V.E. Demidov, M.P. Kostylev, B. Hillebrands, and A.N. Slavin, Phys. Rev. Lett. **93**, 047201 (2004).

[62] A.V. V. Chumak, T. Neumann, A.A.A. Serga, B. Hillebrands, and M.P.P. Kostylev, J. Phys. D. Appl. Phys. **42**, 205005 (2009).

[63] A.V. Chumak, A.A. Serga, and B. Hillebrands, Nat. Commun. **5**, 4700 (2014).

[64] T. Schneider, A.A. Serga, B. Leven, B. Hillebrands, R.L. Stamps, and M.P. Kostylev, Appl. Phys. Lett. **92**, 022505 (2008).

[65] K.S.K.-S. Lee and S.-K.S.K. Kim, J. Appl. Phys. **104**, 053909 (2008).

[66] S. Klingler, P. Pirro, T. Brächer, B. Leven, B. Hillebrands, and A.V. Chumak, Appl. Phys. Lett. **105**, 152410 (2014).

[67] K. Wagner, A. Kákay, K. Schultheiss, A. Henschke, T. Sebastian, and H. Schultheiss, Nat. Nanotechnol. **11**, 432 (2016).

[68] S.J. Hämäläinen, M. Madami, H. Qin, G. Gubbiotti, and S. van Dijken, Nat. Commun. **9**, 4853 (2018).

[69] M. Jamali, J.H. Kwon, S.-M. Seo, K.-J. Lee, and H. Yang, Sci. Rep. **3**, 3160 (2013).

[70] A. Haldar, D. Kumar, and A.O.A.O. Adeyeye, Nat. Nanotechnol. **11**, 437 (2016).

[71] A. Haldar and A.O. Adeyeye, Appl. Phys. Lett. **116**, 162403 (2020).

[72] K. Vogt, F.Y. Fradin, J.E. Pearson, T. Sebastian, S.D. Bader, B. Hillebrands, A. Hoffmann, and H. Schultheiss, Nat. Commun. **5**, 3727 (2014).

[73] K. Vogt, H. Schultheiss, S. Jain, J.E. Pearson, A. Hoffmann, S.D. Bader, and B. Hillebrands, Appl. Phys. Lett. **101**, 042410 (2012).

[74] A. Haldar, C. Tian, and A.O. Adeyeye, Sci. Adv. **3**, e1700638 (2017).

[75] E. Albisetti, D. Petti, M. Pancaldi, M. Madami, S. Tacchi, J. Curtis, W.P. King, A. Papp, G. Csaba, W. Porod, E. Riedo, and R. Bertacco, Nat. Nanotechnol. **11**, 545 (2016).

[76] G. Duerr, K. Thurner, J. Topp, R. Huber, and D. Grundler, Phys. Rev. Lett. **108**, 227202 (2012).

[77] O. Rousseau, M. Yamada, K. Miura, S. Ogawa, and Y. Otani, J. Appl. Phys. **115**, 53914 (2014).

[78] V.E. Demidov, J. Jersch, S.O. Demokritov, K. Rott, P. Krzysteczko, and G. Reiss, Phys. Rev. B **79**, 54417 (2009).

[79] V.E. Demidov, M.P. Kostylev, K. Rott, J. Mnchenberger, G. Reiss, and S.O. Demokritov, Appl. Phys. Lett. **99**, 8 (2011).

[80] V.E. Demidov, S.O. Demokritov, D. Birt, B. O'Gorman, M. Tsoi, and X. Li, Phys. Rev. B - Condens. Matter Mater. Phys. **80**, 0144295 (2009).

[81] T. Schneider, A.A. Serga, A.V. Chumak, C.W. Sandweg, S. Trudel, S. Wolff, M.P. Kostylev, V.S. Tiberkevich, A.N. Slavin, and B. Hillebrands, Phys. Rev. Lett. **104**, 197203 (2010).

[82] X. Xing, Y. Zhou, and H.B. Braun, Phys. Rev. Appl. **13**, 34051 (2020).

[83] M.P. Kostylev, G. Gubbiotti, J.-G. Hu, G. Carlotti, T. Ono, and R.L. Stamps, Phys. Rev. B **76**, 54422 (2007).

[84] V.E. Demidov and S.O. Demokritov, IEEE Trans. Magn. **51**, (2015).

[85] V.E. Demidov, S.O. Demokritov, K. Rott, P. Krzysteczko, and G. Reiss, Phys. Rev. B - Condens. Matter Mater. Phys. **77**, 064406 (2008).

[86] D.R. Birt, B. O'Gorman, M. Tsoi, X. Li, V.E. Demidov, and S.O. Demokritov, Appl. Phys. Lett. **95**, 122510 (2009).

[87] P. Pirro, T. Brächer, K. Vogt, B. Obry, H. Schultheiss, B. Leven, and B. Hillebrands, Phys. Status Solidi Basic Res. **248**, 2404 (2011).

[88] P. Clausen, K. Vogt, H. Schultheiss, S. Schäfer, B. Obry, G. Wolf, P. Pirro, B. Leven, and B. Hillebrands, Appl. Phys. Lett. **99**, 162505 (2011).

[89] F. Garcia-Sanchez, P. Borys, R. Soucaille, J.-P. Adam, R.L. Stamps, and J.-V. Kim, Phys. Rev. Lett. **114**, 247206 (2015).

[90] L. Wang, L. Gao, L. Jin, Y. Liao, T. Wen, X. Tang, H. Zhang, and Z. Zhong, AIP Adv. **8**, 055103 (2018).

[91] P. Pirro, T. Brächer, A.V. V. Chumak, B. Lägel, C. Dubs, O. Surzhenko, P. Görnert, B. Leven, and B. Hillebrands, Appl. Phys. Lett. **104**, 012402 (2014).

[92] T. Sebastian, Y. Ohdaira, T. Kubota, P. Pirro, T. Brächer, K. Vogt, A.A. Serga, H. Naganuma, M. Oogane, Y. Ando, and B. Hillebrands, Appl. Phys. Lett. **100**, 112402 (2012).

[93] S.A. Nikitov, P. Tailhades, and C.S. Tsai, J. Magn. Magn. Mater. **236**, 320 (2001).

[94] A.V. Chumak, V.I. Vasyuchka, A.A. Serga, M.P. Kostylev, V.S. Tiberkevich, and B. Hillebrands, Phys. Rev. Lett. **108**, 257207 (2012).

[95] A.V. Chumak, V.S. Tiberkevich, A.D. Karenowska, A.A. Serga, J.F. Gregg, A.N. Slavin, and B. Hillebrands, Nat. Commun. **1**, 141 (2010).

[96] H. Yu, G. Duerr, R. Huber, M. Bahr, T. Schwarze, F. Brandl, and D. Grundler, Nat. Commun. **4**, 2702 (2013).

[97] Z.K.K. Wang, V.L.L. Zhang, H.S.S. Lim, S.C.C. Ng, M.H.H. Kuok, S. Jain, and A.O.O. Adeyeye, Appl. Phys. Lett. **94**, 083112 (2009).

[98] M. Krawczyk and H. Puszkarski, Phys. Rev. B - Condens. Matter Mater. Phys. **77**, 054437 (2008).

[99] S. Tacchi, G. Duerr, J.W. Klos, M. Madami, S. Neusser, G. Gubbiotti, G. Carlotti, M. Krawczyk, and D. Grundler, Phys. Rev. Lett. **109**, 137202 (2012).

[100] M. Krawczyk and D. Grundler, J. Phys. Condens. Matter **26**, 123202 (2014).

[101] A.V. V. Chumak, A.A.A. Serga, and B. Hillebrands, J. Phys. D. Appl. Phys. **50**, 244001 (2017).

[102] A.V. V. Chumak, P. Pirro, A.A.A. Serga, M.P.P. Kostylev, R.L.L. Stamps, H. Schultheiss, K. Vogt, S.J.J. Hermsdoerfer, B. Laegel, P.A.A. Beck, B. Hillebrands, P.A.A. Beck, and B. Hillebrands, Appl. Phys. Lett. **95**, 262508 (2009).

[103] S. Klingler, P. Pirro, T. Brächer, B. Leven, B. Hillebrands, and A.V. V. Chumak, Appl. Phys. Lett. **106**, 1 (2015).

[104] L. LANDAU and E. LIFSHITZ, Perspect. Theor. Phys. **169**, 51 (1992).

[105] T.L. Gilbert, IEEE Trans. Magn. **40**, 3443 (2004).

[106] B.A. Kalinikos, IEE Proc. H Microwaves, Opt. Antennas **127**, 4 (1980).

[107] B.A. Kalinikos and A.N. Slavin, J. Phys. C Solid State Phys. **19**, 7013 (1986).

[108] G. Gurevich and A. Melkov, *Magnetization Oscillations and Waves* (CRC Press, 1996).

[109] A. Prabhakar and D.D. Stancil, *Spin Waves* (Springer US, 2009).

[110] S.M. Rezende, *Fundamentals of Magnonics* (Springer, 2020).

[111] K.Y. Guslienko and A.N. Slavin, Phys. Rev. B **72**, 14463 (2005).

[112] R.W.W. Damon and J.R.R. Eshbach, J. Phys. Chem. Solids **19**, 308 (1961).

[113] S.O. Demokritov and V.E. Demidov, IEEE Trans. Magn. **44**, 6 (2008).

[114] T. Sebastian, K. Schultheiss, B. Obry, B. Hillebrands, and H. Schultheiss, Front. Phys. **3**, 1 (2015).

[115] M. Madami, G. Gubbiotti, S. Tacchi, and G. Carlotti, *Application of Microfocused Brillouin Light Scattering to the Study of Spin Waves in Low-Dimensional Magnetic Systems*, 1st ed. (Elsevier Inc., 2012).

[116] V.E. Demidov, M.P. Kostylev, K. Rott, P. Krzysteczko, G. Reiss, and S.O. Demokritov, Appl. Phys. Lett. **95**, (2009).

[117] T. Schneider, A.A. Serga, T. Neumann, B. Hillebrands, and M.P. Kostylev, Phys. Rev. B - Condens. Matter Mater. Phys. **77**, 214411 (2008).

[118] H.J.J. Liu, G.A. Riley, and K.S. Buchanan, IEEE Magn. Lett. **6**, 4000304 (2015).

[119] H. Kurebayashi, O. Dzyapko, V.E. Demidov, D. Fang, A.J. Ferguson, and S.O. Demokritov, Appl. Phys. Lett. **99**, 162502 (2011).

[120] T. Brächer, P. Pirro, A.A. Serga, and B. Hillebrands, Appl. Phys. Lett. **103**, 142415 (2013).

[121] T. Schwarze, R. Huber, G. Duerr, and D. Grundler, Phys. Rev. B **85**, 134448 (2012).

[122] G. Consolo, L. Lopez-Diaz, B. Azzerboni, I. Krivorotov, V. Tiberkevich, and A. Slavin, Phys. Rev. B **88**, 14417 (2013).

[123] L.J. Cornelissen, J. Liu, R.A. Duine, J.B. Youssef, and B.J. Van Wees, Nat. Phys. **11**, 1022 (2015).

[124] C.W. Sandweg, Y. Kajiwara, A.V. Chumak, A.A. Serga, V.I. Vasyuchka, M.B. Jungfleisch, E. Saitoh, and B. Hillebrands, Phys. Rev. Lett. **106**, 216601 (2011).

[125] B.L. Giles, Z. Yang, J.S. Jamison, and R.C. Myers, Phys. Rev. B - Condens. Matter Mater. Phys. **92**, 224415 (2015).

[126] A. Haldar and A.O. Adeyeye, Appl. Phys. Lett. **106**, 032404 (2015).

[127] A. Haldar and A.O. Adeyeye, ACS Nano **10**, 1690 (2016).

[128] Q. Wang, B. Heinz, R. Verba, M. Kewenig, P. Pirro, M. Schneider, T. Meyer, B. Lägel, C. Dubs, T. Brächer, and A. V Chumak, Phys. Rev. Lett. **122**, 247202 (2019).

[129] M. Evelt, V.E.E. Demidov, V. Bessonov, S.O.O. Demokritov, J.L.L. Prieto, M. Muñoz, J. Ben Youssef, V.V. V. Naletov, G. de Loubens, O. Klein, M. Collet, K. Garcia-Hernandez, P. Bortolotti, V. Cros, A. Anane, M. Collet, K. Garcia-Hernandez, P. Bortolotti, V. Cros, and A. Anane, Appl. Phys. Lett. **108**, 172406 (2016).

[130] K. Ando, S. Takahashi, K. Harii, K. Sasage, J. Ieda, S. Maekawa, and E. Saitoh, Phys. Rev. Lett. **101**, 036601 (2008).

[131] A. Ganguly, R.M. Rowan-Robinson, A. Haldar, S. Jaiswal, J. Sinha, A.T. Hindmarch, D.A. Atkinson, and A. Barman, Appl. Phys. Lett. **105**, 112409 (2014).

[132] Z. Wang, Y. Sun, Y.Y. Song, M. Wu, H. Schultheib, J.E. Pearson, and A. Hoffmann, Appl. Phys. Lett. **99**, 162511 (2011).

List of figures:

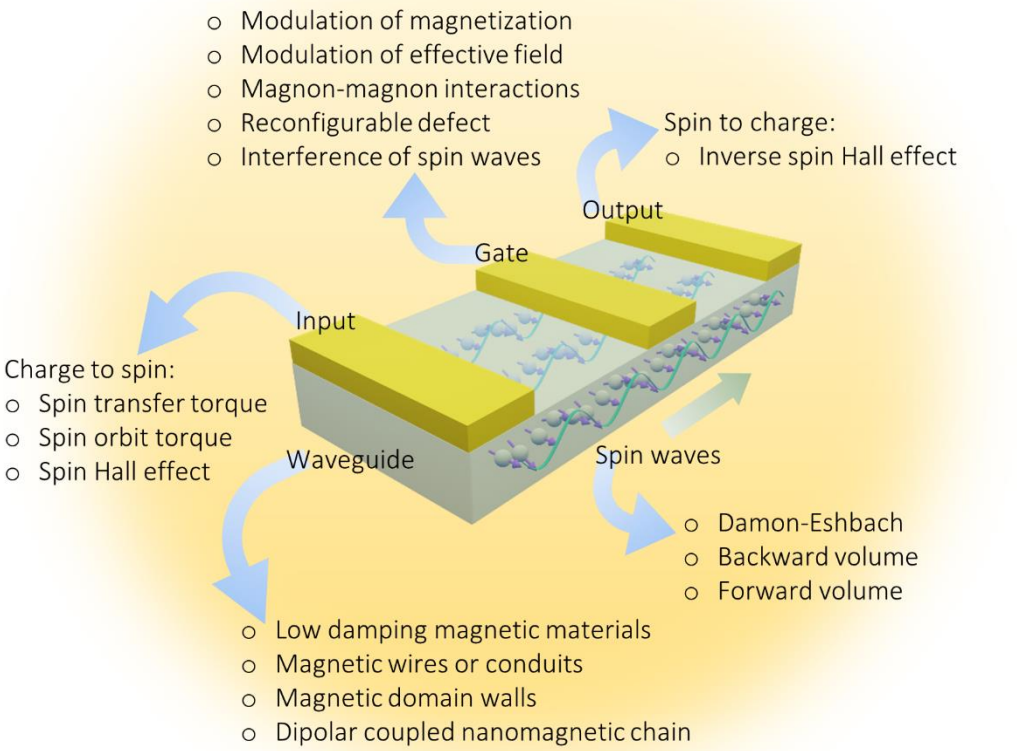

FIGURE 1: Schematic of a magnonic device and its building blocks which are associated with a range of phenomena.

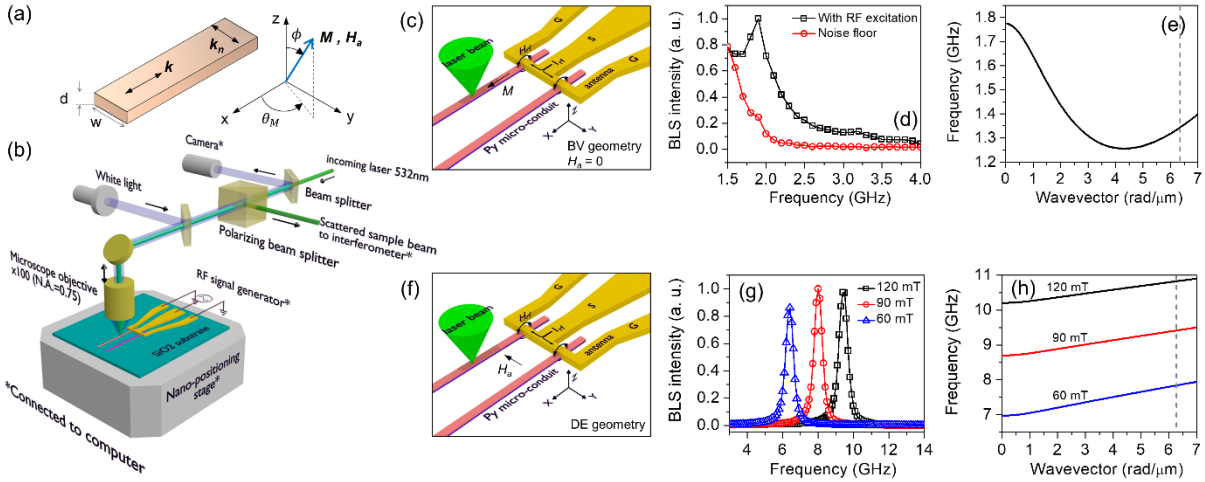

FIGURE 2: (a) Co-ordinate system for the magnetic waveguide and the spin wave propagation. (b) Schematic of the μ-BLS technique. (c) Schematic of the BV geometry with magnetic waveguides with a microwave antenna. (d) BLS spectra recorded at remanence for a Py waveguide where the magnetization is along the length of the waveguide, i.e. BV geometry. (e) Calculated dispersion plot for Py at remanence in the BV spin waves. (f) Schematic of the DE geometry with the field applied along the width of the waveguide. (g) BLS spectra recorded in DE geometry at different fields. (h) Calculated dispersion plot for the DE spin waves at different applied fields. The dotted lines represent the maximum wavevector that can be excited by the 1-μm-wide antenna. Reproduced with permission from Haldar *et al.*, Sci. Adv. **3**, e1700638 (2017). Copyright 2017 Science.

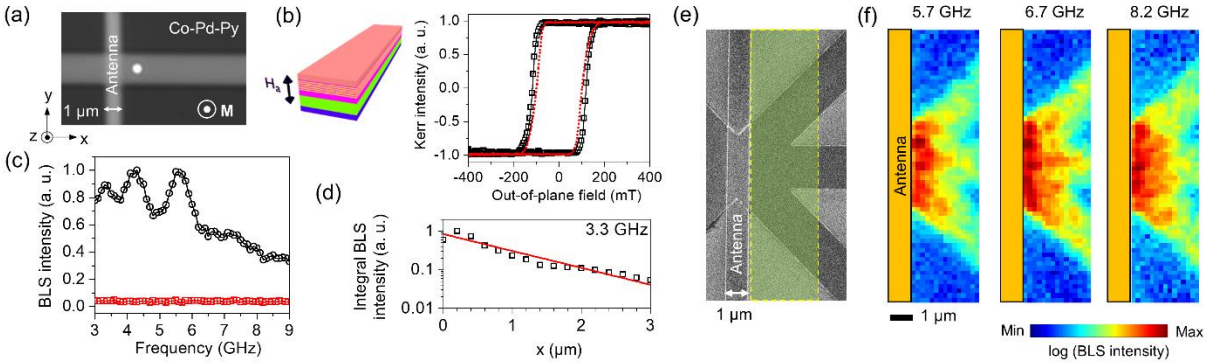

FIGURE 3: (a) BLS camera image of the device where the circular laser spot can be seen. (b) MOKE hysteresis loop for the Co-Pd-Py waveguide when the field was applied in the OOP direction as shown in left schematic. The dotted line in the hysteresis plot refers to a reference thin film. Different colors across the thickness represent the multilayer configuration. (c) BLS spectra recorded at the laser spot position at remanence. The straight line refers to the noise floor recorded without RF excitation. (d) Dependence of spin wave intensity on the propagation coordinate (*x*-axis). (e) SEM image of a waveguide with three channels. (f) 2D spatial image of the spin wave intensity for the modes at 5.7 GHz, 6.7 GHz and 8.2 GHz which exist in all the channels of the waveguide. Reproduced with permission from Haldar *et al*., Sci. Adv. **3**, e1700638 (2017). Copyright 2017 Science.

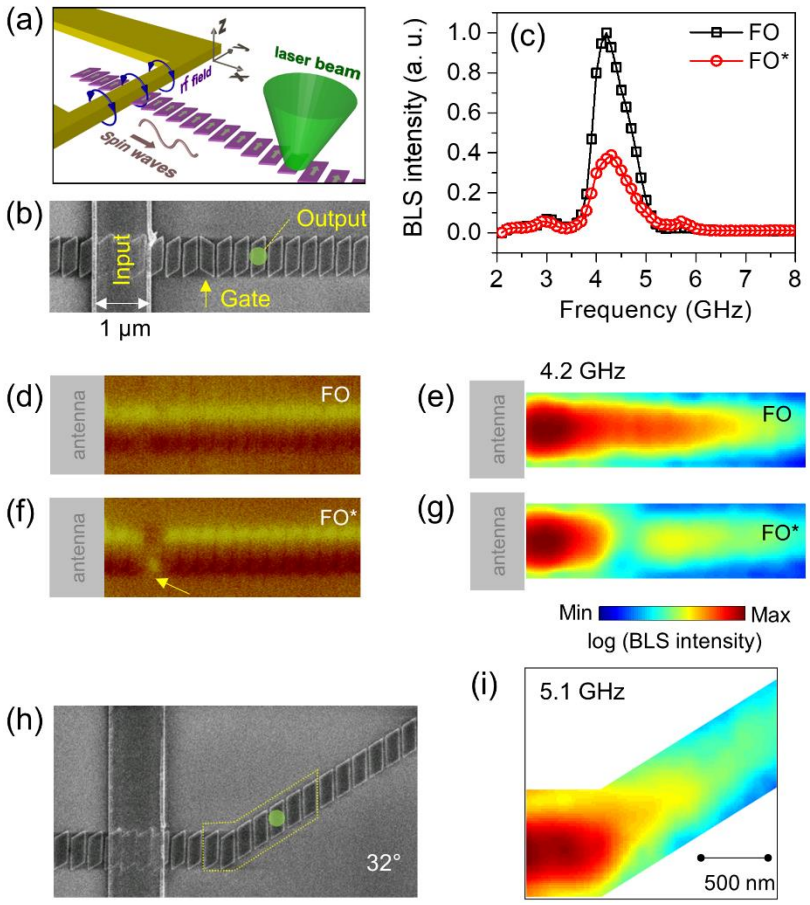

FIGURE 4: Schematic of RNM based waveguide including a microwave antenna and μ-BLS laser spot. (b) SEM image of the RNM waveguide and the antenna fabricated from Py and Pt, respectively. (c) BLS spectra at remanence for the FO (all the RNMs point in the same direction) and FO* (RNM at the 'gate' position has an opposite orientation than other RNMs) state of the waveguide. (d) MFM image showing all the RNMs point in the same direction (FO state) for initialization along their long axis. (e) 2D spatial profile of the spin wave intensity for the FO state. (f) MFM image of the FO* state where the RNM at the 'gate' position has an opposite orientation than other RNMs when initialized along their short axes. (g) 2D spatial map of the spin wave intensity for the FO* state. (h) SEM image of a waveguide with 32° bend. (i) 2D spatial map of the spin wave intensity for the waveguide with 32° bend. Reproduced with permission from Haldar *et al*., Nat. Nanotech. **11**, 437 (2017). Copyright 2016 Nature.

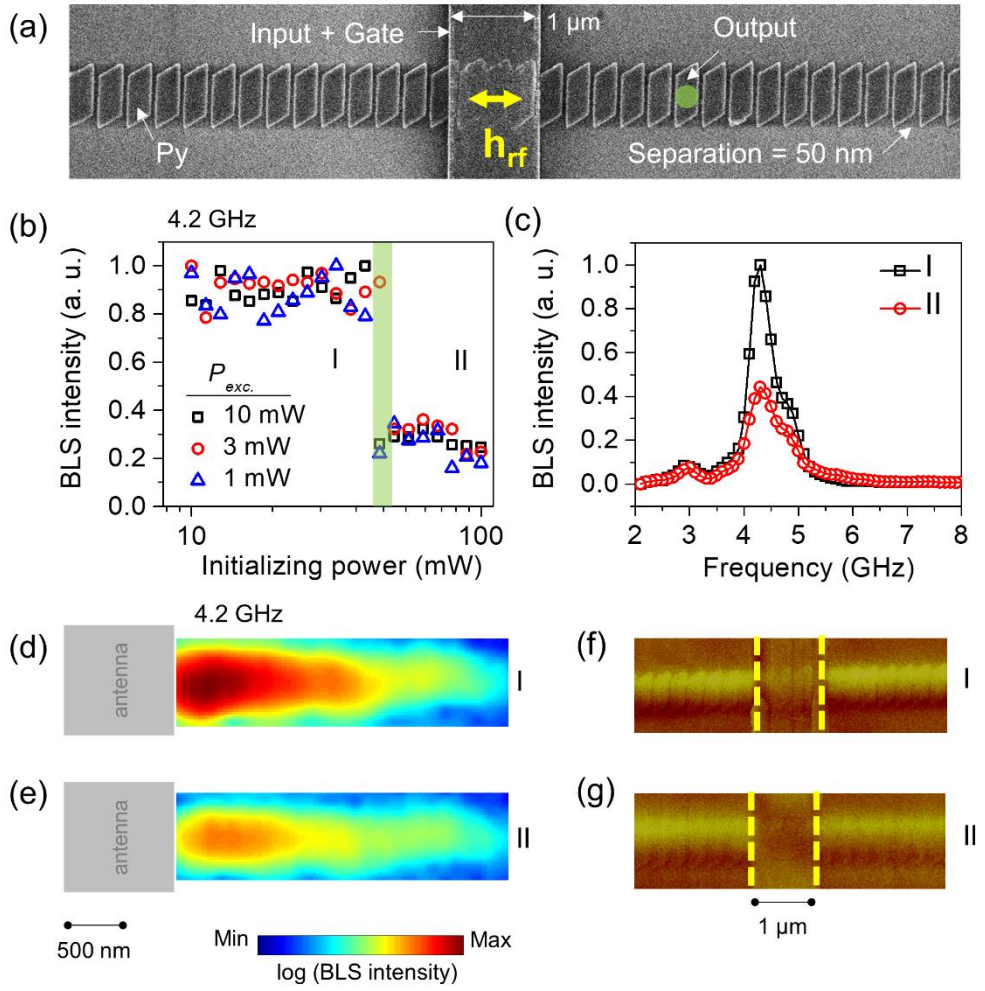

FIGURE 5: (a) SEM image of the waveguide based on RNMs along with an antenna which is used both for spin excitation (input) and manipulation (gate). (b) BLS intensity at 4.2 GHz as a function of microwave initializing power. High intensity and low intensity regions are marked by regions I and II, respectively. Note the log scale for the *x*-axis. (c) Representative BLS spectra for two different initialization regions. (d-e) 2D spatial maps of the spin wave intensity at 4.2 GHz measured by scanning the laser spot for the two different initialization regions. (f-g) MFM images for the two different initialization regions. Reproduced with permission from A. Haldar and A. O. Adeyeye, Appl. Phys. Lett. **116**, 162403 (2020). Copyright 2020 AIP Publishing LLC.